

**SYNTHESIS, STRUCTURAL AND ANTIOXIDANT  
STUDIES OF SOME NOVEL BENZOFURAN AND  
PHTHALIMIDE DERIVATIVES**

**THEN LI YEE**

**UNIVERSITI SAINS MALAYSIA**

**2018**

**SYNTHESIS, STRUCTURAL AND ANTIOXIDANT  
STUDIES OF SOME NOVEL BENZOFURAN AND  
PHTHALIMIDE DERIVATIVES**

by

**THEN LI YEE**

**Thesis submitted in fulfilment of the requirements for  
the degree of  
Master of Science**

**August 2018**

## ACKNOWLEDGEMENT

I am eternally grateful that there are a lot of people who have guided and helped me during my research study. Therefore, I would like to grab this opportunity to express my thankfulness for them throughout this period.

Foremost, I would like to express my deepest respect and gratitude to my supervisor, Assoc. Prof. Dr. Quah Ching Kheng for his supervision, support and encouragement throughout the research journey. Besides, I would like to express my appreciation to Dr. C. S. Chidan Kumar for his assistance and guidance on synthesis works.

With this opportunity, I would like to thanks Ministry of Higher Education Malaysia and Universiti Sains Malaysia for financial support under MyBrain 15 scholarship and USM Fellowship scheme, respectively. In addition, I would like to thank all staffs and labmates from X-ray Crystallography Lab USM for their guidance and support.

Last but not least, I would like to pay my high regards to my family and friends for their patience, support and encouragement for all the time.

## TABLE OF CONTENTS

<b>ACKNOWLEDGEMENT</b> .....	ii
<b>TABLE OF CONTENTS</b> .....	iii
<b>LIST OF TABLES</b> .....	vii
<b>LIST OF FIGURES</b> .....	viii
<b>LIST OF ABBREVIATIONS</b> .....	xiii
<b>ABSTRAK</b> .....	xiv
<b>ABSTRACT</b> .....	xv

### CHAPTER 1 – INTRODUCTION

1.1	X-ray Crystallography .....	1
1.2	Literature Review on Benzofuran Derivatives .....	2
1.3	Literature Review on Phthalimide Derivatives .....	3
1.4	Problem Statement.....	4
1.5	Research Objectives .....	5

### CHAPTER 2 – THEORY

2.1	X-ray Crystallography .....	6
2.1.1	What is a Crystal .....	7
2.1.2	How X-ray Diffraction Determines the Crystal Structure .....	8
2.1.3	The Difference between Real and Reciprocal Space .....	10
2.1.4	Atomic Scattering Factors.....	11
2.1.5	Structure Factors .....	12
2.1.6	Where are the Missing Reflections .....	14

2.1.7	Fourier Transform .....	15
2.1.8	Structure Solution by Direct Methods .....	16
2.1.9	Crystal Structure Refinement.....	17
2.1.10	Molecular Disorder .....	18
2.2	Spectroscopy .....	19
2.2.1	Fourier Transform Infrared (FT-IR) spectroscopy.....	20
2.2.2	Nuclear Magnetic Resonance (NMR) spectroscopy .....	22
2.3	Antioxidant.....	26
2.3.1	Diphenyl-2-picrylhydrazyl (DPPH) Radical Scavenging Assay .....	27
2.3.2	Ferrous Ion Chelating (FIC) Assay .....	28
2.3.3	Hydrogen Peroxide (H <sub>2</sub> O <sub>2</sub> ) Radical Scavenging Assay.....	29

### CHAPTER 3 – INSTRUMENTATIONS AND METHODOLOGY

3.1	Instrumentations and Software Overview .....	30
3.2	X-ray Diffractometer .....	31
3.2.1	Hardware Overview .....	31
3.2.2	Software Overview.....	34
3.2.2 (a)	APEX2 Suite .....	34
3.2.2 (b)	SHELXTL Software Package.....	35
3.3	Sample Preparation.....	36
3.3.1	General Procedure for the Synthesis of 2-(Benzofuran-2-yl)-2-oxoethyl Benzoate (Compounds <b>1a-1q</b> ) .....	37
3.3.2	General Procedure for the Synthesis of 2-((Pyridin-2-ylamino)methyl)isoindoline-1,3-dione (Compounds <b>2a-2g</b> ).....	37
3.3.3	Crystallization .....	37
3.4	Spectroscopic Studies.....	38

3.5	X-ray Analysis.....	54
3.5.1	Crystal Selection .....	54
3.5.2	Crystal Mounting and Alignment .....	55
3.5.3	Data Collection .....	56
3.5.4	Data Reduction and Structure Determination .....	58
3.6	Antioxidant Studies .....	58
3.6.1	Diphenyl-2-picrylhydrazyl (DPPH) Radical Scavenging Assay .....	59
3.6.2	Ferrous Ion Chelating (FIC) Assay .....	59
3.6.3	Hydrogen Peroxide (H <sub>2</sub> O <sub>2</sub> ) Radical Scavenging Assay.....	60

#### **CHAPTER 4 – RESULTS AND DISCUSSIONS**

4.1	Benzofuran Derivatives (Compounds <b>1a-1q</b> ) .....	61
4.1.1	Spectroscopy (FT-IR, <sup>1</sup> H-NMR and <sup>13</sup> C-NMR) .....	61
4.1.2	X-ray Diffraction Data Collection and Refinement.....	63
4.1.3	Crystal Structure Description of Compounds <b>1a-1q</b> .....	68
4.1.4	Antioxidant properties.....	94
4.2	Phthalimide Derivatives (Compounds <b>2a-2g</b> ).....	97
4.2.1	Spectroscopy (FT-IR, <sup>1</sup> H-NMR and <sup>13</sup> C-NMR) .....	97
4.2.2	X-ray Diffraction Data Collection and Refinement.....	99
4.2.3	Crystal Structure Description for Compounds <b>2a-2g</b> .....	101
4.2.4	Antioxidant properties.....	111

#### **CHAPTER 5 – CONCLUSION AND FURTHER STUDIES**

5.1	Benzofuran Moiety .....	112
5.2	Phthalimide Moiety .....	113

5.3 Further Studies ..... 114

**REFERENCES**..... 115

**LIST OF PUBLICATIONS**

## LIST OF TABLES

	<b>Page</b>	
Table 2.1	The 7 crystal systems and 14 Bravais lattices	8
Table 2.2	Rules for general absences	14
Table 2.3	Absence rules for 2 <sub>1</sub> screw axes	15
Table 2.4	Absence rules for glide planes	15
Table 4.1	Crystal data of benzofuran derivatives ( <b>1a-1q</b> )	64
Table 4.2	Torsion angles $\tau_1$ , $\tau_2$ and $\tau_3$ for compounds <b>1a-1q</b>	69
Table 4.3	Hydrogen bond geometries (D—H···A; Å, °) for compounds <b>1a-1q</b>	91
Table 4.4	$\pi\cdots\pi$ interactions in benzofuran compounds	93
Table 4.5	Inhibition results of benzofuran compounds on different assays, including the reference drugs	94
Table 4.6	The IC <sub>50</sub> values of compounds <b>1a</b> , <b>1d</b> , <b>1g</b> and <b>1p</b> , with ascorbic acid as standard drug	95
Table 4.7	Crystal data and structure refinement parameters of phthalimide derivatives ( <b>2a-2g</b> )	99
Table 4.8	Torsion angles $\tau_1$ , $\tau_2$ and $\tau_3$ for compounds <b>2a-2g</b>	102
Table 4.9	Angle between N1—C9—N2 (°) for seven compounds as compared to previous structures	102
Table 4.10	Hydrogen bond geometries (D—H···A; Å, °) for compounds <b>2a-2g</b>	111
Table 4.11	$\pi\cdots\pi$ interactions in compounds <b>2b</b> , <b>2e</b> , <b>2f</b> and <b>2g</b>	111



## LIST OF FIGURES

		<b>Page</b>
Figure 1.1	Chemical structure of benzofuran	2
Figure 1.2	Chemical structure of phthalimide	3
Figure 2.1	The process of X-ray crystallography ( <i>The Structures of Life</i> , 2011)	6
Figure 2.2	The concept of crystal structure	7
Figure 2.3	An example of unit cell	7
Figure 2.4	Schematic cross section of an X-ray tube (Poppe <i>et al.</i> , 2001)	9
Figure 2.5	X-ray diffraction obeying Bragg's law	10
Figure 2.6	Relationship between real lattice and reciprocal lattice (Ooi, 2010)	11
Figure 2.7	Atomic scattering factors for (a) stationary atom, $f_j, \theta$ and (b) temperature-corrected atom, $f_j, \theta, T_j, \theta$ (Ladd & Palmer, 1993)	12
Figure 2.8	Structure factor, $F_{hkl}$ is plotted on an Argand diagram in terms of its amplitude $F_{hkl}$ (represented by the length OF) and resultant phase angle ( $\alpha_{hkl}$ ) (Ladd & Palmer, 1993)	14
Figure 2.9	Fourier connection between real space and reciprocal space	16
Figure 2.10	An example of disorder is shown with odd orientations observed in periodic arrangement	19
Figure 2.11	Electromagnetic spectrum and their respective molecular effects (Wade, 2006)	20
Figure 2.12	The approximate regions where various common types of bonds absorb (only stretching vibrations included for clarity) (Pavia <i>et al.</i> , 1979)	20
Figure 2.13	Vibrational modes of a chemical bond (Pavia <i>et al.</i> , 1979)	21

Figure 2.14	An example of FT-IR spectrum (from own data)	22
Figure 2.15	A simplified correlation chart for proton chemical shift values (Pavia <i>et al.</i> , 1979)	24
Figure 2.16	A simple correlation chart for $^{13}\text{C}$ chemical shift values (Pavia <i>et al.</i> , 1979)	25
Figure 2.17	An example of $^1\text{H}$ -NMR (above) and $^{13}\text{C}$ -NMR (below) spectra (from own data)	26
Figure 2.18	Interactive figure showing difference between normal atom, free radical and antioxidant ( <i>How molecular hydrogen helps to remove Toxic Free Radicals?</i> , 2017)	27
Figure 2.19	Mechanism of DPPH assay	28
Figure 2.20	Ferrozine binds with ferrous ion ( $\text{Fe}^{2+}$ ) to form ferrozine- $\text{Fe}^{2+}$ complex (Hirayama & Nagasawa, 2017)	29
Figure 3.1	Flow chart of research methodology	30
Figure 3.2	Schematic diagram of Bruker APEX II diffractometer ( <i>APEX2 User Manual Version 1.27</i> , 2005)	32
Figure 3.3	Goniometer modules ( <i>APEX2 User Manual Version 1.27</i> , 2005)	32
Figure 3.4	The APEX2 software diagram ( <i>APEX2 User Manual Version 1.27</i> , 2005)	35
Figure 3.5	Crystals formed in a beaker (naked eyes view)	55
Figure 3.6	Crystal mounted on a copper pin is aligned, with the help of a video microscope	56
Figure 3.7	Intensity spots of a crystalline sample in a diffraction frame	56
Figure 3.8	The deviation histograms show whether the crystal sample is single (left hand side) or multiple (right hand side)	57
Figure 4.1	General chemical diagram of seventeen benzofuran derivatives, showing torsion angles $\tau_1$ , $\tau_2$ and $\tau_3$	68
Figure 4.2	<i>ORTEP</i> diagram of compound <b>1a</b> with 30% ellipsoid probability and atomic labelling scheme	70
Figure 4.3	Hydrogen bonds (cyan dotted lines) joined molecules into a wave-like chain in compound <b>1a</b>	71

Figure 4.4	C—H $\cdots$ $\pi$ interactions (blue double dotted lines) in compound <b>1a</b>	71
Figure 4.5	Molecular structures of compounds <b>1b-1e</b> drawn at 30% ellipsoid probability with atomic labelling scheme	72
Figure 4.6	Dimeric structure formed by two inversion-related molecules in compounds <b>1b</b> and <b>1c</b>	73
Figure 4.7	Packing diagram of <b>1b</b> and <b>1c</b> viewed along <i>a</i> -axis, showing hydrogen bondings (cyan dotted lines) and $\pi\cdots\pi$ interactions (red dotted lines)	74
Figure 4.8	Molecular structure of compound <b>1d</b> , with disorder part shown in purple colour	75
Figure 4.9	Partial packing diagram of <b>1d</b> view along (a) <i>b</i> -axis and (b) <i>a</i> -axis with disorder molecules <i>B'</i> presented in purple colour	76
Figure 4.10	A hydrogen bonded chain of compound <b>1e</b> directing along <i>b</i> -axis	77
Figure 4.11	Hydrogen bonds (cyan dotted lines) and $\pi\cdots\pi$ interactions (red dotted lines) stack molecules into two dimensional plates in compound <b>1e</b>	77
Figure 4.12	Molecular structure of compounds <b>1f-1h</b> drawn at 30% ellipsoid probability with suitable atomic labelling scheme	78
Figure 4.13	Extensive interactions in compounds <b>1f</b> and <b>1g</b> , including hydrogen bonds (cyan dotted lines), C—H $\cdots$ $\pi$ interactions (blue dotted lines) and $\pi\cdots\pi$ interactions (red dotted lines)	79
Figure 4.14	Molecules in <b>1g</b> are joined by hydrogen bonds to form one-dimensional chain, with atom C5 serves as bifurcated donor	79
Figure 4.15	Partial packing of compound <b>1h</b> shown along <i>b</i> -axis, with blue dotted lines indicating C—H $\cdots$ $\pi$ interactions and red dotted lines indicating $\pi\cdots\pi$ interactions	80
Figure 4.16	Molecular structures of compounds <b>1i</b> , <b>1j</b> and <b>1k</b> in <i>ORTEP</i> style with 30% ellipsoid probability and atomic labelling scheme	81
Figure 4.17	An inversion dimer-dimer chain formed by extensive hydrogen bonds in compound <b>1i</b>	82

Figure 4.18	Molecular packing of compound <b>1i</b> participated by hydrogen bonds (cyan dotted lines), C—H··· $\pi$ interactions (blue dotted lines) and $\pi$ ··· $\pi$ interactions (red dotted lines)	82
Figure 4.19	Partial packing diagram of compounds <b>1j</b> and <b>1k</b> , showing hydrogen bonds (cyan dotted lines), C—H··· $\pi$ interactions (blue dotted lines) and $\pi$ ··· $\pi$ interactions (red dotted lines)	83
Figure 4.20	<i>ORTEP</i> structure of compounds <b>1l</b> , <b>1m</b> and <b>1n</b> drawn at 30% ellipsoid probability with suitable atomic labelling	84
Figure 4.21	Molecules in compound <b>1l</b> are organized into fishbone sheets in alternate up-down manner	85
Figure 4.22	Molecular packing of compound <b>1m</b> viewed along [010] direction	85
Figure 4.23	$\pi$ ··· $\pi$ interactions in compound <b>1n</b> are displayed in (a) <i>bc</i> -view and (b) <i>ab</i> -view, showing molecules <i>A</i> (in purple) and molecules <i>B</i> (in green)	86
Figure 4.24	Compounds <b>1o-1q</b> are presented in <i>ORTEP</i> style with 30% ellipsoid probability and atomic labelling scheme	87
Figure 4.25	Compound <b>1o</b> with a <i>S</i> (6) ring motif formed by intramolecular hydrogen bond	88
Figure 4.26	Molecular packing of compound <b>1o</b> , showing hydrogen bonds (cyan dotted lines) and $\pi$ ··· $\pi$ interactions (red dotted lines)	88
Figure 4.27	Molecular disorder in compound <b>1p</b> , showing molecule <i>B</i> and disordered molecule <i>Y</i> (purple colour)	89
Figure 4.28	Partial packing diagram of compound <b>1p</b> , showing disordered molecules (purple colour) and solvent molecules (green colour), with hydrogen bonds (cyan dotted lines) and $\pi$ ··· $\pi$ interactions (red dotted lines)	89
Figure 4.29	Partial packing of compound <b>1q</b> as viewed along <i>b</i> -axis	90
Figure 4.30	IC <sub>50</sub> values for H <sub>2</sub> O <sub>2</sub> radical scavenging activity of compounds <b>1a</b> , <b>1d</b> , <b>1g</b> and <b>1p</b> in comparison with the standard drug (ascorbic acid)	96
Figure 4.31	General chemical diagram of <b>2a-2g</b> , showing three characteristic torsion angles ( $\tau_1$ , $\tau_2$ and $\tau_3$ )	101
Figure 4.32	<i>ORTEP</i> diagram of <b>2a-2g</b> with 30% ellipsoid probability and atomic labelling scheme	103

Figure 4.33	Hydrogen bonds connect inversion-related molecules into dimeric chain in (a) compound <b>2a</b> and (b) compound <b>2c</b>	104
Figure 4.34	Packing diagram of (a) compound <b>2a</b> and (b) compound <b>2c</b> as viewed along <i>a</i> -axis	105
Figure 4.35	Hydrogen bonds (cyan dotted lines) and $\pi \cdots \pi$ interaction (red dotted lines) in the molecular packing of compound <b>2b</b>	106
Figure 4.36	Partial packing diagram of compound <b>2d</b> as viewed along <i>a</i> -axis with dimeric structure shown at enlarged view	107
Figure 4.37	Molecular interactions in molecular packing of compound <b>2e</b> , showing C—H $\cdots$ O hydrogen bonds (cyan dotted lines), C—H $\cdots$ $\pi$ interactions (blue dotted lines) and $\pi \cdots \pi$ interactions (red dotted lines)	108
Figure 4.38	Dimers are joined by hydrogen bonds to form column along [100] direction	108
Figure 4.39	The intermolecular C—H $\cdots$ O hydrogen bonds in compound <b>2f</b> join molecules into endless chain	109
Figure 4.40	Partial packing diagram of <b>2f</b> viewed along <i>a</i> -axis, showing C—H $\cdots$ $\pi$ interactions (blue dotted lines) and $\pi \cdots \pi$ interactions (red dotted lines)	109
Figure 4.41	Dimeric structure in compound <b>2g</b> , showing intramolecular and intermolecular hydrogen bonds (cyan dotted lines)	110
Figure 4.42	The packing structure of compound <b>2g</b> as viewed along <i>b</i> -axis	110

## LIST OF ABBREVIATIONS

<b>3D</b>	Three-dimensional
<b>IUPAC</b>	International Union of Pure and Applied Chemistry
<b>CSD</b>	Cambridge Structural Database
<b>wR</b>	Weighted Reliability Index
<b>R</b>	Reliability Index
<b>S</b>	Goodness of fit
<b>FT-IR</b>	Fourier Transform Infrared
<b>NMR</b>	Nuclear Magnetic Resonance
<b>DPPH</b>	Diphenyl-2-picrylhydrazyl
<b>FIC</b>	Ferrous Ion Chelating
<b>H<sub>2</sub>O<sub>2</sub></b>	Hydrogen peroxide
<b>ATR</b>	Attenuated total reflection
<b>SMART</b>	Siemens Molecular Analysis Research Tools
<b>CCD</b>	Charge-Coupled Device
<b>BIS</b>	Bruker Instrument Service
<b>GUI</b>	Graphical User Interface
<b>ORTEP</b>	Oak Ridge Thermal Ellipsoid Plot
<b>TLC</b>	Thin-layer chromatography
<b>IC<sub>50</sub></b>	Half maximal inhibitory concentration

# SINTESIS, KAJIAN STRUKTUR DAN ANTIOKSIDAN BEBERAPA TERBITAN BENZOFURAN DAN FTALIMIDA BARU

## ABSTRAK

Dalam projek ini, dua siri analog heterosiklik yang mengandungi bahagian benzofuran (**1a-1q**) dan ftalimida (**2a-2g**) telah disintesis dan dihablurkan. Semua struktur hablur telah ditunjukkan melalui teknik kristalografi sinar-X hablur tunggal, disokong oleh analisis spektrum FT-IR dan NMR. Struktur molekul dan interaksi dalam sebatian ini telah dikaji dan dianalisis. Selain itu, potensi antioksidan semua sebatian telah dinilai menggunakan asai antioksidan yang berlainan. Dalam siri benzofuran, lapan daripada tujuh belas sebatian terbentuk dalam kumpulan ruang triklinik  $P\bar{1}$ , lima dalam monoklinik  $P2_1/n$ , dua dalam monoklinik  $C2/c$ , manakala dua dalam ortorombik  $Pna2_1$  dan  $P2_12_12_1$ . Penghubung  $C-C(=O)-C-O-C(=O)$  dalam molekul benzofuran ini mengambil konformasi yang hampir berserenjang ataupun hampir mendatar. Interaksi antara molekul paling banyak diperhatikan dalam sebatian **1f-1k** manakala paling kurang dalam sebatian **1c** dan **1n**. Didapati bahawa sebatian **1a**, **1d**, **1g** dan **1p** aktif terhadap asai pelupusan radikal  $H_2O_2$  dengan penambahan gantian penyumbang elektron. Dalam siri ftalimida, lima daripada tujuh sebatian mengambil kumpulan ruang triklinik  $P\bar{1}$  manakala dua mempamerkan monoklinik  $P2_1/c$  dan  $P2_1/n$ . Secara ketara, konfigurasi berbentuk V dapat dilihat dalam semua struktur, merujuk kepada sudut  $N1-C9-N2$  mereka. Dalam padatan molekul, kebanyakan interaksi dapat diperlihatkan dalam sebatian **2f** manakala paling sedikit dalam sebatian **2d**. Berdasarkan keputusan penghambatan, adalah didapati bahawa sebatian (**2a-2g**) tidak aktif terhadap kajian antioksidan.

**SYNTHESIS, STRUCTURAL AND ANTIOXIDANT STUDIES OF SOME  
NOVEL BENZOFURAN AND PHTHALIMIDE DERIVATIVES**

**ABSTRACT**

In this project, two series of heterocyclic analogues bearing a benzofuran (**1a-1q**) and a phthalimide (**2a-2g**) moieties were synthesized and crystallized. All crystal structures were revealed by single crystal X-ray crystallography technique, supported by FT-IR and NMR spectral analysis. The molecular structures and interactions of these compounds were studied and analysed. Besides, the antioxidant potential of all compounds were evaluated using different antioxidant assays. In the benzofuran series, eight of seventeen compounds are assembled in a triclinic  $P\bar{1}$  space group, five in monoclinic  $P2_1/n$ , two in monoclinic  $C2/c$ , whereas two in orthorhombic  $Pna2_1$  and  $P2_12_12_1$ . The C—C(=O)—C—O—C(=O) connecting bridge of these benzofuran molecules tends to adopt a nearly perpendicular or a nearly planar conformation. Intermolecular interactions are most observable in compounds **1f-1k** while the least in compounds **1c** and **1n**. It was found that compounds **1a**, **1d**, **1g** and **1p** were active towards H<sub>2</sub>O<sub>2</sub> radical scavenging assay, with the incorporation of electron donating substituents. In the phthalimide series, five from seven compounds adopt a triclinic  $P\bar{1}$  space group while two exhibit monoclinic  $P2_1/c$  and  $P2_1/n$ . Significantly, a V-shaped configuration is observed in all structures, with respects to their N1—C9—N2 angles. In the molecular packing, most interactions are observed in compound **2f** whereas the least in compound **2d**. Based on the inhibition results, it was found that compounds (**2a-2g**) are antioxidant inactive.



## CHAPTER 1

### INTRODUCTION

#### 1.1 X-ray Crystallography

X-ray crystallography is a scientific way used to explore the internal structure of a crystal through its atomic arrangement by X-ray diffraction. By computing the diffracting beams of various intensities from the crystal lattice, scientists could build a three-dimensional (3D) model showing the molecular structure of a compound. This method contributes to many areas including chemistry, pharmacology, molecular biology, materials science and mineralogy. It is the most comprehensive method available to study the molecular structure of a compound, providing fundamental information for molecular design and other structural-related studies. However, this method has its limitation because a good crystal is needed to get precision crystallographic structure in which the process of crystallization is not an ease (Deschamps, 2010).

X-ray crystallography has been introduced and continuously improved since more than a hundred years ago. X-rays were discovered in 1895 and systematically studied by William Conrad Röntgen, a German physicist who won the first Nobel Prize in Physics in 1901. Years later, another German physicist, Max von Laue found that X-ray will be scattered in certain directions when interacting with a crystal. The phenomenon is known as X-ray diffraction. This discovery awarded him a Nobel Prize in Physics in 1914 (Schneegans, 2014). The father and son team, William Henry Bragg and William Lawrence Bragg further investigated the properties of X-rays after Laue's discovery. The elder Bragg believed that X-rays should have particle nature but the younger Bragg agreed with Laue that X-rays are waves. The young Bragg proposed that reflected X-rays might tell the arrangement of atoms in a crystal. Hence, he

developed a simple mathematical equation to explain the diffraction of X-rays, which is known as Bragg's Law. Owing to their great contributions in X-ray crystallography, the Bragg duo were awarded the Nobel Prize in Physics in the year 1915 (Bragg, William Lawrence, 2009).

As time goes by, more and more crystal structures are revealed and the time taken to determine a crystal structure is getting shorter thanks to the continuing advances in every aspects of X-ray diffraction procedure.

## 1.2 Literature Review on Benzofuran Derivatives

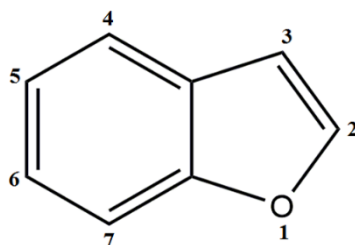


**Figure 1.1** Chemical structure of benzofuran.

Oxygen-containing heterocyclic compounds are common structural elements of many bioactive structures. Benzofuran (IUPAC name: 1-Benzofuran) (Figure 1.1) is one of these heterocycles and it is composed of a fused benzene and furan (Furan, 2012) ring. The benzofuran and its derivatives present abundantly in nature because they are stable and easy to generate, especially those with substitution(s) at their C-2 and/or C-3 (Coşkun *et al.*, 2016, Shankerrao *et al.*, 2017) positions. Numerous natural benzofuran derivatives have been isolated from plants (Naik *et al.*, 2015) as well as marine sources (Jin *et al.*, 2016) as this privilege structure (DeSimone *et al.*, 2004) possess a broad range of biological activities as well as pharmacological profiles. Some of these biological and medicinal significance such as antioxidant, antimicrobial, anticancer and antiviral were described and reported in review articles (Khanam & Shamsuzzaman, 2015, Nevagi *et al.*, 2015, Heravi *et al.*, 2017, Chand *et al.*, 2017), which in turn verify the value of this moiety in medicinal chemistry. These noteworthy

potentials of benzofuran ring system and its derivatives have generated the curiosity in researchers to explore this scaffold more deeply. Despite the strenuous and time consuming isolation method, synthetic chemists were inspired to synthesize some newly compounds incorporating this core structure, with some modifications on its skeleton. Besides biological properties, benzofuran derivatives also serve as building blocks for cosmetic formulations (Leung & Foster, 1996), fluorescent sensors (Higashi *et al.*, 2017) and optical brighteners (Siegrist *et al.*, 2003).

### 1.3 Literature Review on Phthalimide Derivatives

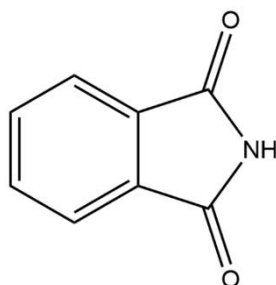


**Figure 1.2** Chemical structure of phthalimide.

Diverse biological profiles have been revealed for phthalimide (Figure 1.2) and its analogs (Kushwaha & Kaushik, 2016, Sharma *et al.*, 2010). The phthalimide (IUPAC name: Isoindole-1,3-dione) is one of the nitrogen containing heterocycles. The skeleton of the phthalimide core consists of a fused benzene and maleimide (*Maleimide*, 2018) ring. The imide functional group ( $\text{—CO—N(H)—CO—}$ ) is hydrophobic and neutral, thus it can penetrate biological membranes *in vivo*, and is playing a vital role in enhancing biological reactions (Bansode *et al.*, 2009). The structural miscellany and biological importance of this *N*-heterocycle make it a vital character in the design of new prototypes of drug candidates. Thalidomide (Mujagic *et al.*, 2002, Calabrese & Fleischer, 2000), one of the famous derivatives of phthalimide, was once applied as a sedative, but then inhibited from the market owing to its teratogenic effects in 1960s. However, it has drawn back the attention of

researchers thanks to its potential uses in the treatment of various diseases such as leprosy, tuberculosis, angiogenesis and human immunodeficiency virus (HIV) infections. The phthalimide synthon exhibits good antioxidant (Chidan Kumar *et al.*, 2015), anticonvulsant (Abdel-Hafez, 2004), anti-inflammatory (Machado *et al.*, 2005), analgesic (Fhid *et al.*, 2014) and immunomodulatory (Cardoso *et al.*, 2015) properties. In industry, phthalimide analogues are broadly contributed as herbicides (Natsume *et al.*, 1997), dyes (Koh *et al.*, 2008), heat resistant polymers (Nasirtabrizi *et al.*, 2013) and flame-retardants (Bohen *et al.*, 1990). These aforementioned results prompted us to choose phthalimide core in the synthesis of some new compounds to investigate more on its structure as well as potentials.

#### **1.4 Problem Statement**

Heterocyclic compounds are gaining attentions as their physical and chemical properties are revolutionized distinctively with the presence of a heteroatom (Katritzky, 2014). Significantly, the structure of heterocyclic compounds such as benzofuran and phthalimide, can be manipulated to unlock more functions by introducing different functional groups as substituent or as a part of their rings (Arora *et al.*, 2012). To authenticate the modified structures, structure determination is crucial where X-ray crystallography method is so far the most precise, non-destructive method to determine the three-dimensional structure of a compound. Investigation on the crystal structure provides information about molecular geometries and interactions as well as the spatial arrangements of molecules within a crystal. By understanding the structural behaviours of a compound, assisted by database such as Cambridge Structural Database (CSD) for literature reference, structure-based drug design is much more efficient even at atomic-level (Lionta *et al.*, 2014). Excessive free radicals in human body may cause oxidative damage to cells and lead to pathophysiological

changes. People nowadays are more concern on health care and have lifelong desire to delay aging process. Therefore, scientists are motivated to discover safer and multipotent antioxidant agents to inhibit these harms since early stage (Karthik *et al.*, 2015). Henceforth, the goal of this research is to study the crystal structure of newly prepared pharmacological active compounds through single crystal X-ray diffraction and subsequently evaluate their antioxidant potentials.

### **1.5 Research Objectives**

The objectives of this research work are:

- i. To synthesize novel compounds of benzofuran and phthalimide derivatives.
- ii. To elucidate the molecular structure of synthesized compounds by using FT-IR and NMR spectroscopy.
- iii. To examine the crystal structure of synthesized compounds and study their supramolecular features by using X-ray crystallography technique.
- iv. To evaluate the antioxidant potential of newly synthesized compounds.

## CHAPTER 2

### THEORY

In this study, there are several methods used to probe the internal structure of the compounds including X-ray crystallography, FT-IR and NMR spectroscopy. The theory behind these methods are briefly described in this chapter. Besides, types of antioxidant assays used to evaluate the compounds are also presented.

#### 2.1 X-ray Crystallography

Study on the unique arrangement of molecules inside a crystal structure provides us information about connectivity, interactions and conformation as well as bond lengths and angles. Nevertheless, it is impossible to observe a crystal structure with naked eyes, hence crystallographers make use of X-ray diffraction method to ‘see’ it. X-ray diffraction is a process where X-rays hit a crystal, interact with it and scatter. In X-ray crystallography technique (Figure 2.1), these scattered rays superpose to produce diffraction frames bearing structural information of the crystal. The three dimensional crystal structure are revealed *via* electron contour map generated through Fourier transform from diffraction frames.

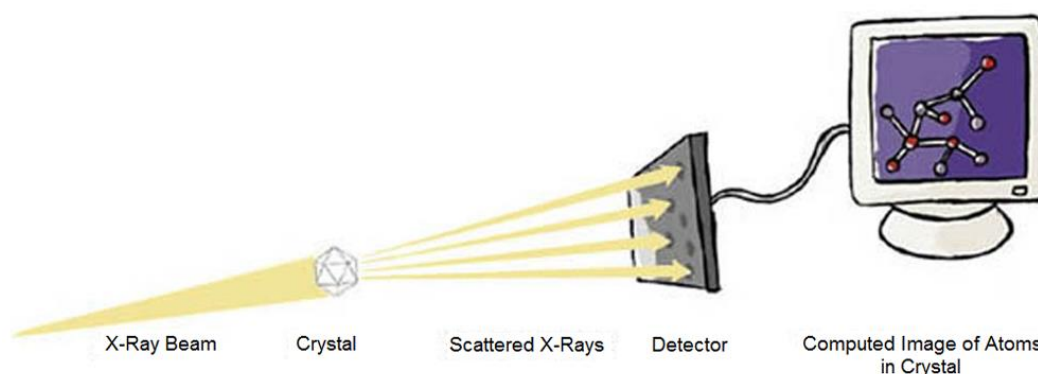


**Figure 2.1** The process of X-ray crystallography (*The Structures of Life*, 2011).

### 2.1.1 What is a Crystal

A crystal appears to be glossy and has flawless edges from exterior most of the time. The clue is, the interior of this solid state matter is made up of periodic arrays of atoms, which can be explained by the idea of lattice and basis (set of atoms) (Figure 2.2).

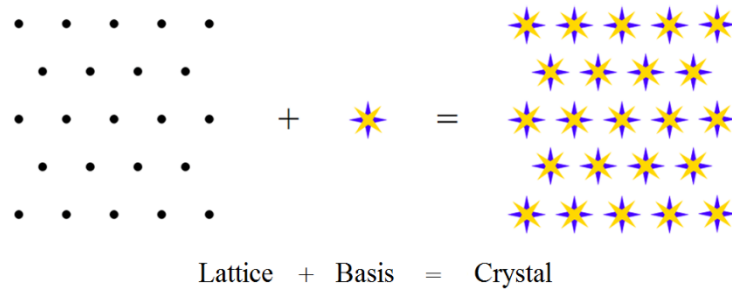


**Figure 2.2** The concept of crystal structure.

A crystal lattice is formed by the smallest repeating building blocks known as the unit cell (Figure 2.3), which with unique cell parameters (cell axes  $a$ ,  $b$  and  $c$ ; inter axial angles  $\alpha$ ,  $\beta$  and  $\gamma$ ), translating throughout the entire crystal in three dimensions. In crystallography, there are 7 crystal systems and 4 lattice types [primitive (P), body-centred (I), face-centred (F) and base-centred (A, B or C)], contributing to a total of 14 possible Bravais lattices, to describe the pattern of molecular packing (Table 2.1).

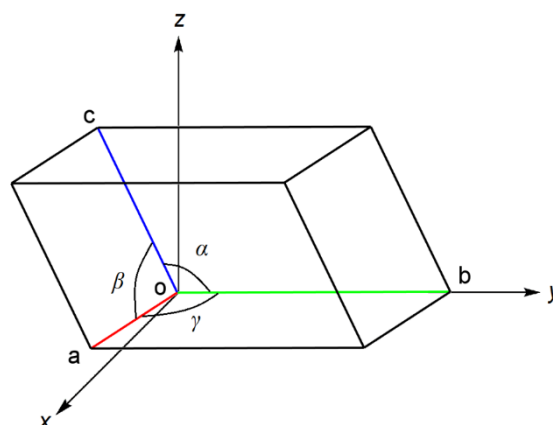


**Figure 2.3** An example of unit cell.

**Table 2.1** The 7 crystal systems and 14 Bravais lattices.

Crystal System	Unit cell axes	Inter axial angles	Bravais lattices
<b>Cubic</b>	$a = b = c$	$\alpha = \beta = \gamma = 90^\circ$	P, I, F
<b>Tetragonal</b>	$a = b \neq c$	$\alpha = \beta = \gamma = 90^\circ$	P, I
<b>Orthorhombic</b>	$a \neq b \neq c$	$\alpha = \beta = \gamma = 90^\circ$	P, I, F; A, B or C
<b>Hexagonal</b>	$a = b \neq c$	$\alpha = \beta = 90^\circ; \gamma = 120^\circ$	P
<b>Trigonal</b>	$a = b \neq c$	$\alpha = \beta = 90^\circ; \gamma = 120^\circ$	P
<b>Monoclinic</b>	$a \neq b \neq c$	$\alpha = \beta = 90^\circ; \gamma \neq 120^\circ$	P, C
<b>Triclinic</b>	$a \neq b \neq c$	$\alpha \neq \beta \neq \gamma \neq 90^\circ$	P

The minimum repeating motifs in a crystal structure (or known as the asymmetric unit) are related by symmetry operations. Combination of different lattice types with various symmetry elements such as reflection, inversion, rotation and *etc.* leads to 230 space groups which were usually denoted by Hermann-Mauguin notation. The Hermann-Mauguin notation is constituted of 4 elements: lattice type followed by symmetry element at each unit cell axis. An example of space group notation is *Pmmm*, describing an orthorhombic crystal with primitive lattice and mirror planes perpendicular to each *a*-, *b*- and *c*-axis.

### 2.1.2 How X-ray Diffraction Determines the Crystal Structure

X-rays are high energy electromagnetic waves with wavelengths range from 0.02 to 100 Å (1 Å equals to  $1 \times 10^{-10}$  m). Its dual nature properties allows it to behave like particles as well as waves. Beforehand, let's have a short overview on the production of X-rays. In an evacuated X-ray tube (Figure 2.4), high speed electrons travel from tungsten filament (cathode) to strike on a pure metal target (anode), which is usually made from molybdenum, copper, tungsten, iron and *etc.* depending on wavelength requirement. The massive impact (due to high voltage) bombards the electrons inside the target to higher energy states. As the excited electron drops back to lower energy state, X-ray radiation is emitted through beryllium windows. During the process, the metal target is always cooled with running water to prevent overheating.



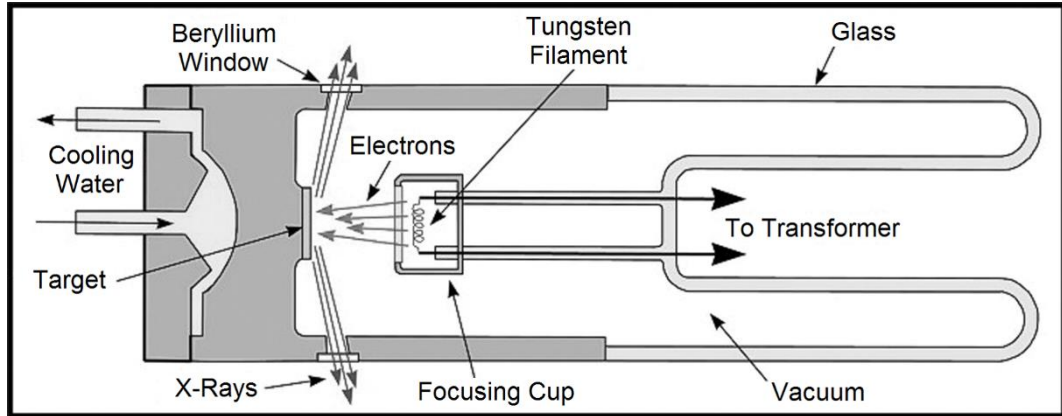


**Figure 2.4** Schematic cross section of an X-ray tube (Poppe *et al.*, 2001).

Crystal lattice is assembled by imaginary planes so-called Miller planes, with Miller indices  $hkl$ , acting as weakly reflecting surfaces (Stoner & Hurst, 2017). When X-rays are directed onto a crystal, they will be reflected (diffracted) to various directions due to the interaction with the electrons surrounding the atoms from each plane. This is possible because the wavelengths of X-rays are comparable to the interatomic separations of solids (about 1 to 3 Å).

The X-ray diffraction by a crystal can be explained using Bragg's law (Figure 2.5). Let the inter planar spacing of Miller planes be  $d$ , when X-rays (ray 1 and ray 2) hit atoms on two adjacent planes at an angle  $\theta$  and are both diffracted away, ray 2 travels an extra path of  $PR + QR$  than ray 1. In order to form a diffraction spot (constructive interference occurs), the path difference between ray 1 and ray 2 must equal to some integer multiple of  $\lambda$  (full wave cycle).

$$\text{Hence,} \quad PR + QR = n\lambda. \quad (2.1)$$

$$\text{From trigonometry,} \quad \sin\theta = PR/d. \quad (2.2)$$

$$\text{Since } PR = QR, \quad PR + QR = 2d\sin\theta. \quad (2.3)$$

$$\text{Therefore,} \quad 2d\sin\theta = n\lambda \text{ (Bragg's law)}. \quad (2.4)$$

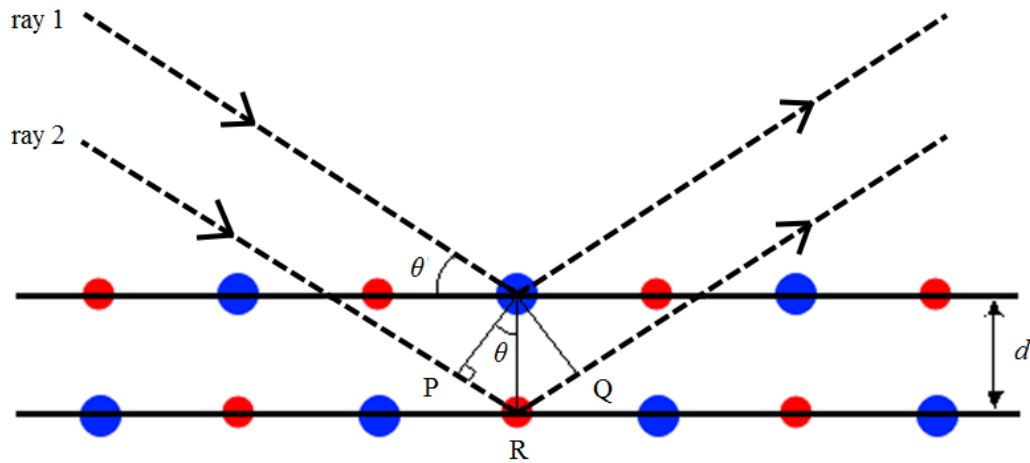


**Figure 2.5** X-ray diffraction obeying Bragg's law.

### 2.1.3 The Difference between Real and Reciprocal Space

Sum of diffractions from each  $d$ -spaced Miller plane (real lattice) corresponds to a point in reciprocal lattice, which are recorded as diffraction frames throughout the experiment. The diffraction pattern (in units of  $1/d$ ) can be described by rearranging the Bragg's law equation, which is  $2d\sin\theta = n\lambda$  to become  $\sin\theta = \left(\frac{n\lambda}{2}\right)\left(\frac{1}{d}\right)$ , *i.e.* the larger the  $d$  spacing of crystal lattice, the closer the diffraction spots and vice versa. All these diffraction frames are then sorted out to rebuild a diffraction map, which also known as the reciprocal lattice. From the reciprocal space, we only obtain information regarding the intensities and phases of Bragg's peaks. Yet, these allow crystallographers to calculate the electron density map (in real lattice) to determine the absolute crystal structure. From the real space, crystal information such as atomic parameters and molecular geometries could be studied.

In mathematics, real space and reciprocal space are interconnected *via* Fourier transform. Unit cell parameters of both spaces could be represented by Equations 2.5 and 2.6 (\* for reciprocal) (Figure 2.6).

$$a \cdot a^* = b \cdot b^* = c \cdot c^* \quad (2.5)$$

$$\alpha = \alpha^*; \beta = \beta^*; \gamma = \gamma^* \quad (2.6)$$

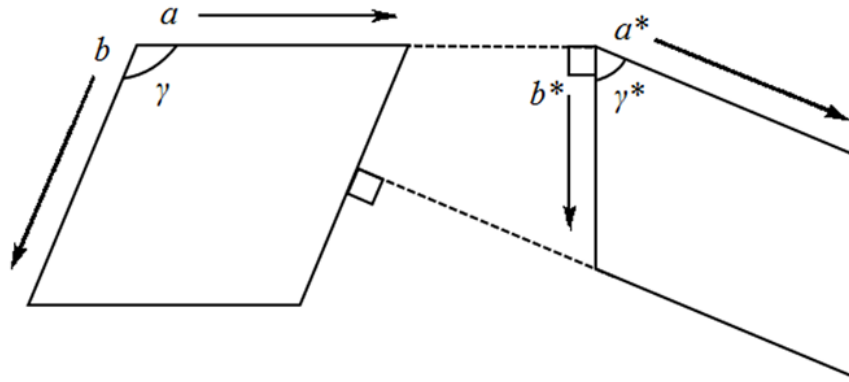


**Figure 2.6** Relationship between real lattice and reciprocal lattice (Ooi, 2010).

### 2.1.4 Atomic Scattering Factors

Every atom is surrounded by its individual electron cloud and hence, the scattering of X-rays by an atom is actually due to interactions between X-rays with electrons. Atomic scattering factor (or atomic form factor),  $f_j$  where  $j$  is the number of electrons, is a measure on scattering efficiency of X-rays waves by an atom compared to a single electron within (Ooi, 2010). Atomic scattering factors are involved in many crystallographic calculations such as structure factor of a given Bragg's peak. The scattering effect of an atom greatly relies on the atomic nature, the direction of scattering, the wavelength of incident radiation and the thermal vibrations of the atom (Ladd & Palmer, 1993). Each element has a unique atomic scattering factor, which is tabulated in the International Tables for X-ray Crystallography, as a function of  $(\sin\theta)/\lambda$ .

For an atom in stationary state, the scattering factor increases with increasing atomic number ( $Z$ ), contradictory light atoms such as hydrogen are usually harder to localize from the diffraction map. Path differences between scattered X-rays become larger for higher Bragg angle and smaller wavelength (Figure 2.7). At zero scattering angle ( $\theta = 0^\circ$ ), the waves are in phase so the scattering amplitude is proportional and maximum to atomic number  $Z$ . However, at higher Bragg angle, more scattering waves

are out of phase hence destructive interferences happens and consequently reduces the intensities of diffraction spots (*Atomic scattering factor*, 2017).

In solid, atoms constantly vibrate about their equilibrium positions unless external energy (for example heat energy) is supplied. Assume all atoms in the crystal vibrate in isotropic manner, the scattering factor for the  $j$ th atom is corrected by

$$T_{j,\theta} = e^{\frac{-B_j \sin^2 \theta}{\lambda^2}} \quad (2.7)$$

where  $B_j$ , which is the temperature factor of atom  $j$ , is given by

$$B_j = 8\pi^2 \overline{U_j^2} \quad (2.8)$$

for that  $\overline{U_j^2}$ , which is a function of temperature, representing the mean-square vibrational amplitude of the  $j$ th atom normal to the reflecting plane from its equilibrium position. Counting in the thermal factor,  $T$  (also function of  $(\sin\theta)/\lambda$ ), the temperature-corrected atomic scattering factor could be expressed as

$$g_j = f_{j,\theta} \cdot T_{j,\theta}. \quad (2.9)$$

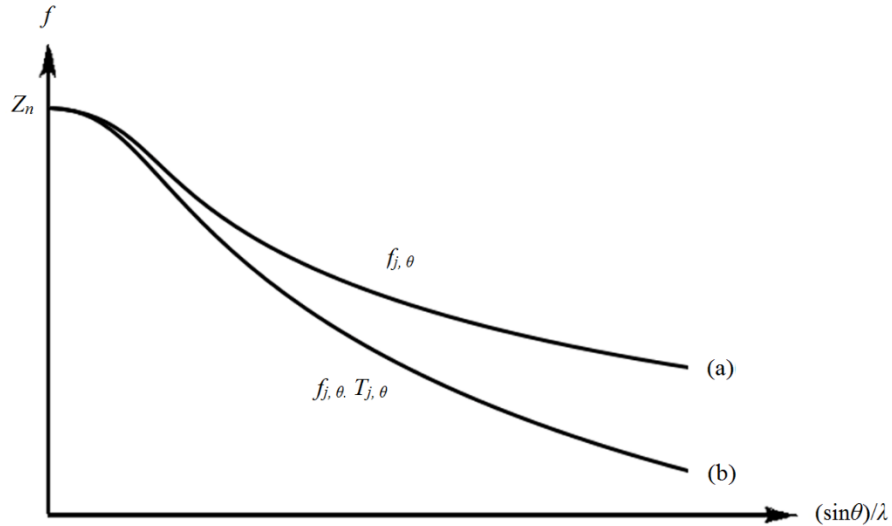


**Figure 2.7** Atomic scattering factors for (a) stationary atom,  $f_{j,\theta}$  and (b) temperature-corrected atom,  $f_{j,\theta} \cdot T_{j,\theta}$  (Ladd & Palmer, 1993).

### 2.1.5 Structure Factors

The intensity,  $I$  of each diffraction spot is integrated and expressed as structure factor,  $F_{hkl}$  where  $I \propto (F_{hkl})^2$ . The structure factor,  $F_{hkl}$ , is a quantity used to express

the amplitude and phase,  $\alpha_{hkl}$ , of diffracted beams from certain Miller planes (*Structure factor*, 2017). The structure factor is influenced by the atomic scattering factors,  $g_j$  and it covers information about the Miller planes as well as the position of respective atoms within the unit cell. It is a vital character in constructing the electron density map for the crystal structure (Ooi, 2010). In the generation of electron density map, structure factors of all diffracted rays from a unit cell are calculated and summated, as a unit cell could represent whole crystal structure *via* translational symmetry.

Let the fractional coordinates of atoms of type  $j$  from an  $hkl$  plane in the examined crystal be  $x_j$ ,  $y_j$  and  $z_j$ , the structure factors can be expressed by Equations 2.10 and 2.11:

$$F_{hkl} = \sum_1^N g_j \exp[i2\pi(hx_j + ky_j + lz_j)] \quad (2.10)$$

$$F_{hkl} = \sum_1^N g_j \cos 2\pi(hx_j + ky_j + lz_j) + i \sum_1^N g_j \sin 2\pi(hx_j + ky_j + lz_j) \quad (2.11)$$

where  $N$  is total number of atoms and  $i$  is the imaginary number,  $\sqrt{-1}$ . An Argand diagram (Figure 2.8) can be used to demonstrate the structure factor in vector form by putting  $\mathbf{A}_{hkl}$  as  $\sum_1^N g_j \cos 2\pi(hx_j + ky_j + lz_j)$  and  $\mathbf{B}_{hkl}$  as  $\sum_1^N g_j \sin 2\pi(hx_j + ky_j + lz_j)$ . Thus, the structure factor equation becomes

$$\mathbf{F}_{hkl} = \mathbf{A}_{hkl} + i\mathbf{B}_{hkl}. \quad (2.12)$$

In this case, the resultant phase angle could be calculated by

$$\alpha_{hkl} = \tan^{-1}(B/A) \quad (2.13)$$

where  $A = |\mathbf{A}|$  (2.14)

and  $B = |\mathbf{B}|$ . (2.15)

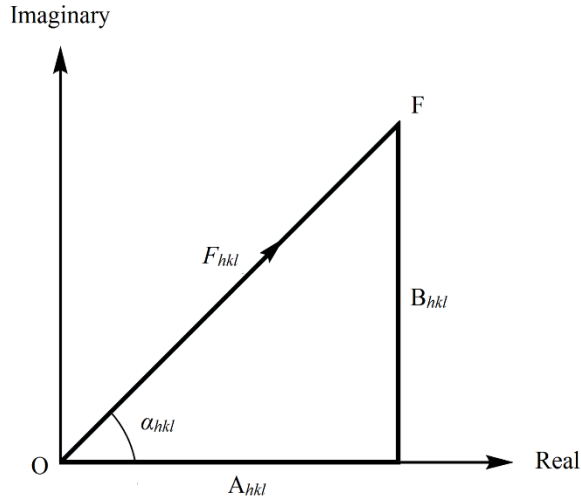


**Figure 2.8** Structure factor,  $F_{hkl}$  is plotted on an Argand diagram in terms of its amplitude  $|F_{hkl}|$  (represented by the length OF) and resultant phase angle ( $\alpha_{hkl}$ ) (Ladd & Palmer, 1993).

### 2.1.6 Where are the Missing Reflections

There are reflections, as well as absences found in a diffraction frame. Absence occurs when diffracted X-rays form destructive interferences from certain Miller planes (structure factor shows a zero value as a result of no intensity). The absence of diffraction spots is essential in determining which space group the crystal adopts. There are two types of absences in crystallography, which are general absences and systematic absences. In essence, the general absences decides the lattice type for a unit cell, based on certain conditions (Table 2.2). For example, a body-centred lattice,  $I$  shows no reflection when the Miller indices from such plane is an odd sum ( $2n+1$ ).

**Table 2.2** Rules for general absences.

Lattice type	Condition for general absences
$P$	None
$A$	$hkl : k + l = 2n+1$
$B$	$hkl : h + l = 2n+1$
$C$	$hkl : h + k = 2n+1$
$I$	$hkl : h + k + l = 2n+1$
$F$	$hkl : \text{Neither all odd nor all even}$

On the other hand, the systematic absences (Table 2.3 and 2.4) reflects the translational symmetry elements (screw axes and glide planes) in a crystal. For

examples, a screw axis along  $a$ -axis only happens in Miller planes of  $(h00)$  when  $h$  is odd and absent; a  $c$ -glide plane perpendicular to  $a$ -axis has no intensity in  $hk0$  planes when  $h$  is odd.

**Table 2.3** Absence rules for  $2_1$  screw axes.

Orientation	Condition for systematic absences
Along $a$ -axis	$h00 : h = 2n+1$
Along $b$ -axis	$0k0 : k = 2n+1$
Along $c$ -axis	$00l : l = 2n+1$

**Table 2.4** Absence rules for glide planes.

Glide plane	Orientation	Condition for systematic absences
$a$ -glide	Perpendicular to $b$ -axis	$0kl : k = 2n+1$
	Perpendicular to $c$ -axis	$0kl : l = 2n+1$
$b$ -glide	Perpendicular to $a$ -axis	$h0l : h = 2n+1$
	Perpendicular to $c$ -axis	$h0l : l = 2n+1$
$c$ -glide	Perpendicular to $a$ -axis	$hk0 : h = 2n+1$
	Perpendicular to $b$ -axis	$hk0 : k = 2n+1$
$n$ -glide	Perpendicular to $a$ -axis	$0kl : k + l = 2n+1$
	Perpendicular to $b$ -axis	$h0l : h + l = 2n+1$
	Perpendicular to $c$ -axis	$hk0 : h + k = 2n+1$

\* $n$ -axis is diagonal axis.

### 2.1.7 Fourier Transform

Each diffracted ray from Miller planes has its own direction, amplitude and phase angle. During data collection, the direction and the amplitude of diffracted X-rays are identified. Unfortunately, there is still no way to measure the incident phase angle,  $\alpha_{hkl}$ , henceforth the phase problem arises.

With the aid of mathematics, real space and reciprocal space could be interrelated *via* Fourier transform since the repeating unit cells in crystal lattice are analogous to a periodic function (Figure 2.9). For a unit cell of volume  $V$ , the electron density,  $\rho_{xyz}$ , at  $(x, y, z)$  coordinate can be denoted by a Fourier equation as

$$\rho_{xyz} = \frac{1}{V} \sum_h \sum_k \sum_l |F_{hkl}| \cos 2\pi(hx + ky + lz - \alpha_{hkl}) \quad (2.16)$$

in unit of electrons per cubic angstroms ( $\text{e}\text{\AA}^{-3}$ ). Through Fourier synthesis (inverse Fourier transform), electron density map comprising atomic parameters are calculated based on structure factors. With these information, the missing phases can be identified by Fourier analysis (forward Fourier transform) (Ooi, 2010).

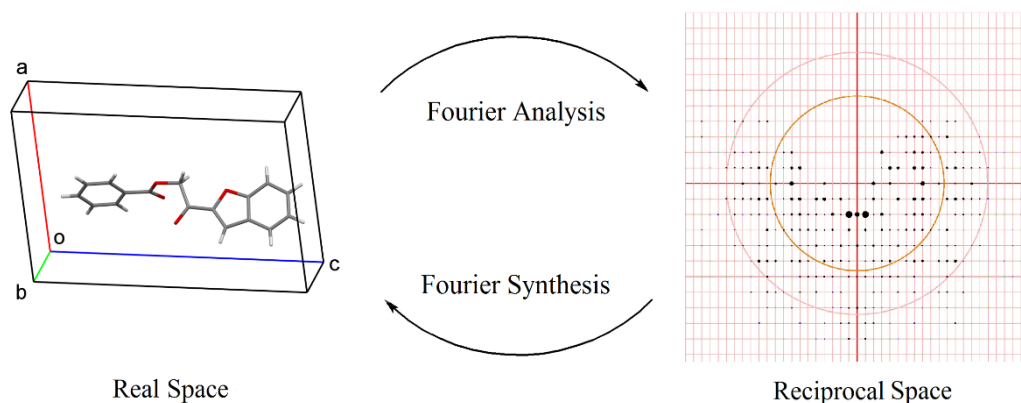


**Figure 2.9** Fourier connection between real space and reciprocal space.

### 2.1.8 Structure Solution by Direct Methods

Structure solution is a process to construct a molecular model for the crystal structure under investigation through calculations. This process also known as phasing, in which the phase problem is going to be solved. Typically, there are two common ways to solve the phase problem, which are direct methods and Patterson methods based on molecule type. Direct methods are basically meant for small organic molecules without heavy atom, whereas Patterson methods often applied on structures with heavy atom.

In this study, direct methods are utilized because the studied compounds are small carbon-based molecules and contain no heavy element. Ultimately, possible phase angles for every diffraction are deduced directly from respective structure factors based on two conditions: (i) the resulting electron density must never be



negative value and (ii) sharp peaks are present only at or near atomic positions and zero peaks elsewhere in an electron density map.

Several steps are included during structure solution by direct methods (Ooi, 2010). The first is to transform structure factors,  $F_{hkl}$  to normalized structure factors,  $E_{hkl}$ . The normalized structure factor excludes the thermal effects on atoms in order to exploit atomic information. It also compensates for the decrease of discrete scattering factors  $f$  with increasing Bragg angles. Only those promising normalized structure factors are obtained through the Equation 2.17,

$$|E_{hkl}| = \frac{|F_{hkl}|}{\sqrt{\varepsilon \sum_{j=1}^N f_j^2}} \quad (2.17)$$

where  $\varepsilon$  is an integer governed by crystal class and type of reflections. The next stage is origin-fixing of a unit cell. Some of the strongest reflections based on  $E_{hkl}$  are assigned with phases as to determine the coordinates for the origin (0, 0, 0) within crystal lattice. Although  $F_{hkl}$  is structure invariants, yet a sign change may occur due to phase changes, hence selection of origin should be thoughtful as this will affect the relative phases for such reflections. Once the origin is fixed, reflections with high  $|E_{hkl}|$  value are examined in triplet sets to compare their phase angles. The sum for each  $h, k, l$  in a triplet set should be equal to zero. Next, the most plausible phase set are employed to develop an  $E_{hkl}$ -based electron density map. Recognizable features of the structure such as benzene rings are first identified as a preliminary testing model. However, the model may still be incomplete and need to be refined in order to get the final absolute crystal structure.

### 2.1.9 Crystal Structure Refinement

The structural model derived from structure solution has to undergo a series of adjustment and enhancement to match the diffraction data, which so-called the

refinement process. For small molecules with atomic number less than 200, least-squares refinement is usually in practise. Instead of the measured (observed) structure factors,  $F_o$ , this method calculates another set of structure factor (calculated),  $F_c$ , and compares both set of values. Every refinement should improve the model quality and this repeat until a minimum deviation between  $F_o$  and  $F_c$  is obtained.

In least-squares refinement, the model's quality is assured by three common residual factors, also known as  $R$ -factors (Sheldrick, 2015). Among them are the weighted residual factor ( $wR$  or  $wR_2$ , based on  $F^2$ ), the unweighted residual factor ( $R$  or  $R_1$ , based on  $F$ ) and the goodness of fit ( $S$ ). The values of  $wR_2$  and  $R$  should converge to a minimum and the equation for both weighted and unweighted  $R$ -factors are shown in Equations 2.18 and 2.19.

$$wR_2 = \left[ \frac{\sum w(F_o^2 - F_c^2)^2}{\sum w(F_o^2)^2} \right]^{1/2} \quad (2.18)$$

$$R = \frac{\sum (|F_o| - |F_c|)^2}{\sum |F_o|} \quad (2.19)$$

The goodness of fit measures how well the experimental structure matches the theoretical structure. The value of  $S$  should close to but not less than unity, else the too perfect model is suspicious. The equation for goodness of fit is expressed below, where  $N_R$  denotes the number of independent reflections and  $N_P$  denotes the number of refined parameters.

$$S = \left[ \frac{\sum w(F_o^2 - F_c^2)^2}{N_R - N_P} \right]^{1/2} \quad (2.20)$$

#### 2.1.10 Molecular Disorder

Once in a while, the periodic orientation in a crystal may exist some differently oriented structures. This phenomenon is known as molecular disorder (Figure 2.10). When molecular disorder occurs, the value of  $R$ -index is higher than usual even all

atoms are correctly assigned. Hence, crystallographers have to identify the residual electron density for these special parts during refinements while the occupancies for normal and disordered components should sum to unity. If succeed, the value of R-index will be minimized.

In general, disorder in a crystal structure can be distinguished into two groups: substitutional disorder and positional disorder (Sheldrick, 2015). Substitutional disorder happens when the same coordinate of two unit cell hosted by different types of atoms. This usually is indicated by unusual value of either anisotropic or isotropic displacement parameters. Positional disorder includes static and dynamic modes, happens when one atom hosts more than one location. In static case, one would see the fusion of two structure conformations at one site and it is much easier to be recognized. For dynamic case, it is harder to be solved because the molecule might always “moving” though the occurring possibility of disorder could be reduced by utilizing low-temperature data collection.

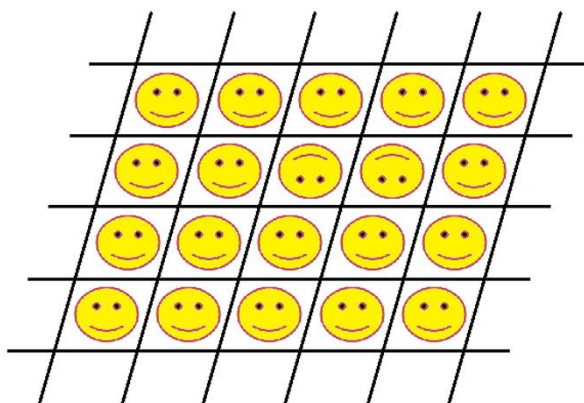



**Figure 2.10** An example of disorder is shown with odd orientations observed in periodic arrangement.

## 2.2 Spectroscopy

Spectroscopy studies the interactions between electromagnetic waves (Figure 2.11) and matter. It is a non-destructive way to discover the structure of a compound, with little amount of sample required, hence greatly employed in organic chemistry.

In this context, two spectroscopic techniques are briefly discussed, which are the Fourier Transform Infrared (FT-IR) spectroscopy and the Nuclear Magnetic Resonance (NMR) spectroscopy (proton and carbon-13).



Higher frequency	Wavelength, $\lambda$ (m)	Region	Molecular effects
	$10^{-11}$	Gamma rays	
	$10^{-9}$	X-rays Vacuum UV	Ionization
	$10^{-7}$	Near UV	
	$10^{-6}$	Visible	Electronic transition
	$10^{-5}$	Infrared	Molecular vibrations
	$10^{-3}$	Microwave	Rotational motion
	$10^0$	Radio	Nuclear spin transition
Lower frequency	$10^2$		

**Figure 2.11** Electromagnetic spectrum and their respective molecular effects (Wade, 2006).

### 2.2.1 Fourier Transform Infrared (FT-IR) spectroscopy

The Fourier Transform Infrared (FT-IR) spectroscopy includes the infrared zone of the electromagnetic spectrum. It deals with the vibrational motions of chemical bonds (only those with changing dipole moment) to authenticate the presence or absence of various functional groups in a molecule (Pavia *et al.*, 1979). In FT-IR spectroscopy, infrared photons are absorbed by molecules near to their natural vibrating frequencies, hence the molecular vibrations are resonated and these signals are recorded as absorption spectrum by the detector (Figure 2.12). The absorption spectrum for each compound is unique, acting as a fingerprint for structural identification.

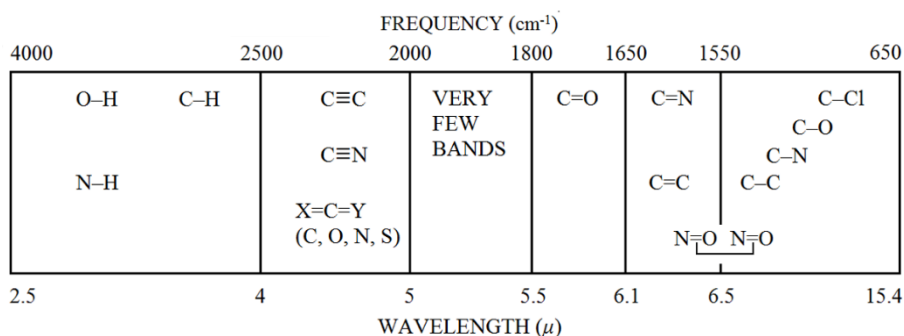


**Figure 2.12** The approximate regions where various common types of bonds absorb (only stretching vibrations included for clarity) (Pavia *et al.*, 1979).

Photon energy,  $E$ , is quantized and depends on its frequency,  $\nu$ , or wavelength,  $\lambda$ , where  $c$  is speed of light and  $h$  is the Planck's constant.

$$E = h\nu \quad (2.21)$$

$$E = \frac{hc}{\lambda} \quad (2.22)$$

Generally, the absorption frequencies in FT-IR spectroscopy are expressed in wavenumber,  $\bar{\nu}$ , which is also the reciprocal of wavelength (in centimeters). This is because wavenumber is easier to interpret and directly proportional to energy, in which a higher wavenumber indicates a higher energy level.

$$\text{wavenumber, } \bar{\nu}(\text{cm}^{-1}) = \frac{1}{\text{wavelength, } \lambda(\text{cm})} \quad (2.23)$$

There are two kinds of vibrational modes in an infrared active molecule, the stretching and bending modes (Figure 2.13). Normally, higher frequencies are observed for stretching vibrations than bending vibrations for a particular bond. Interpretation of FT-IR spectrum (Figure 2.14) could be done by referring to the infrared correlation tables as a guide.

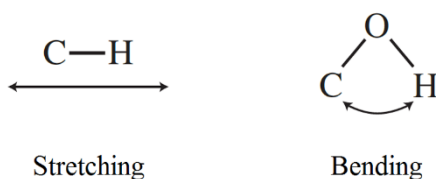


**Figure 2.13** Vibrational modes of a chemical bond (Pavia *et al.*, 1979).

Consider the chemical bond between two atoms as a spring system, the energy of the spring (bond) is determined by its stiffness ( $K$ ) and the masses of the two bonded atoms ( $m_1$  and  $m_2$ ). The natural vibrating frequency of a bond can be estimated from Hooke's law, which is given by

$$\bar{\nu} = \frac{1}{2\pi c} \sqrt{\frac{K}{\mu}} \quad (2.24)$$

where  $K$  is the force constants in dynes/cm and  $\mu$  is the reduced mass of the system expressed as

$$\mu = \frac{m_1 m_2}{m_1 + m_2} \quad (2.25)$$

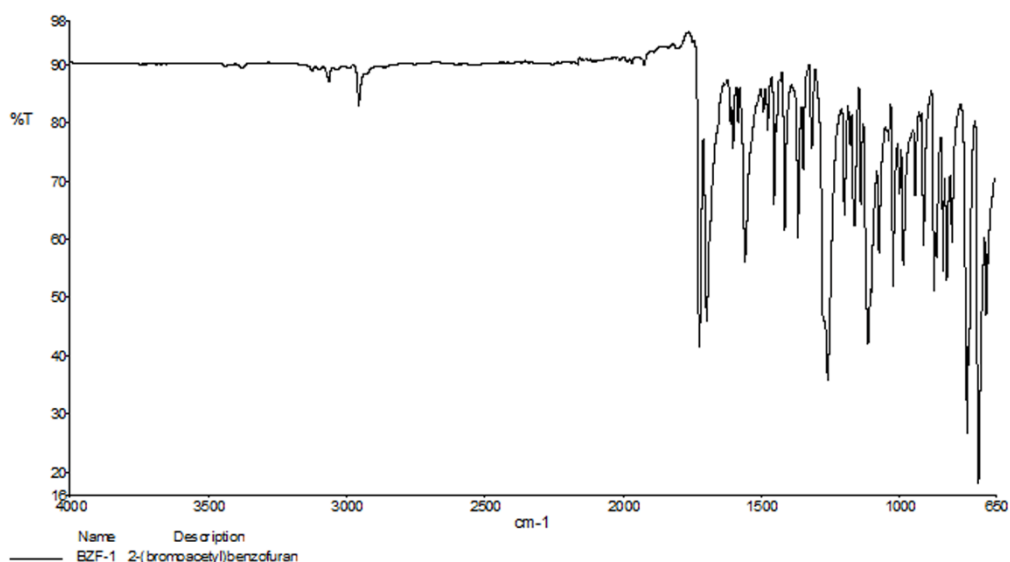


**Figure 2.14** An example of FT-IR spectrum (from own data).

### 2.2.2 Nuclear Magnetic Resonance (NMR) spectroscopy

The Nuclear Magnetic Resonance (NMR) spectroscopy takes place at the radiofrequency zone of the electromagnetic spectrum. It discloses the molecular structure of a compound by studying the local magnetic field around atomic nuclei (Pavia *et al.*, 1979). Most atomic nuclei with odd atomic number or odd mass number such as proton and carbon-13 have nuclear spins. When an atom is positioned inside a magnetic field, the low energy radio waves will only be able to excite its nucleus to cause spin transitions, which are also known as resonance. The NMR signals produced are recorded as peaks in the spectrum.

Energy absorbed to cause a spin change is quantized and equal to the energy difference between the two involved states. For example, a proton atom has two spin states:  $+\frac{1}{2}$  and  $-\frac{1}{2}$ , the energy to induce spin change in proton is given by Equation 2.26:

$$E_{\text{absorbed}} = \left( E_{-\frac{1}{2}\text{state}} - E_{+\frac{1}{2}\text{state}} \right) \quad (2.26)$$

$$= h\nu$$

In NMR spectroscopy, chemical shift,  $\delta$ , is generally used to indicate how much a proton/carbon resonance shifted from the standard, tetramethylsilane (TMS) in part per million (ppm) of the spectrometer's operating frequency. This is due to the slight difference in resonance frequency is hard to detect for a sole compound, thus is compared to a known standard, TMS. The reference value for chemical shift could be found in the chemical shift correlation chart (Pavia *et al.*, 1979) (Figure 2.15 and 2.16).

$$\text{chemical shift, } \delta(\text{ppm}) = \frac{\text{shift (in Hz)}}{\text{spectrometer frequency (in MHz)}} \quad (2.27)$$

In the spectrum of  $^1\text{H-NMR}$  (Figure 2.17), different sets of peaks are exhibited for protons in distinct chemical environment. Conversely, protons that are chemically equivalent may result in a single peak. The area under each peak indicates the amount of protons exists at that position, in the form of area ratio but not absolute number. Since atomic nucleus is surrounded by electrons, the value of chemical shift for every peak is influenced by the shielding effect on the nucleus. Besides individual data, the splitting of peak could provide information on its neighbour with the  $n + 1$  rule. For instance, a proton senses two protons ( $n = 2$ ) attached to its adjacent carbon, hence a triplet ( $2 + 1 = 3$ ) is observed for this proton. The peak separation in a multiplet is defined by their coupling constant,  $J$  (in Hertz), which tells how a nucleus is magnetically affected by its neighbours. Normally, a group of magnetically coupled protons (such as protons in a benzene ring) can be distinguished by their coupling constant.

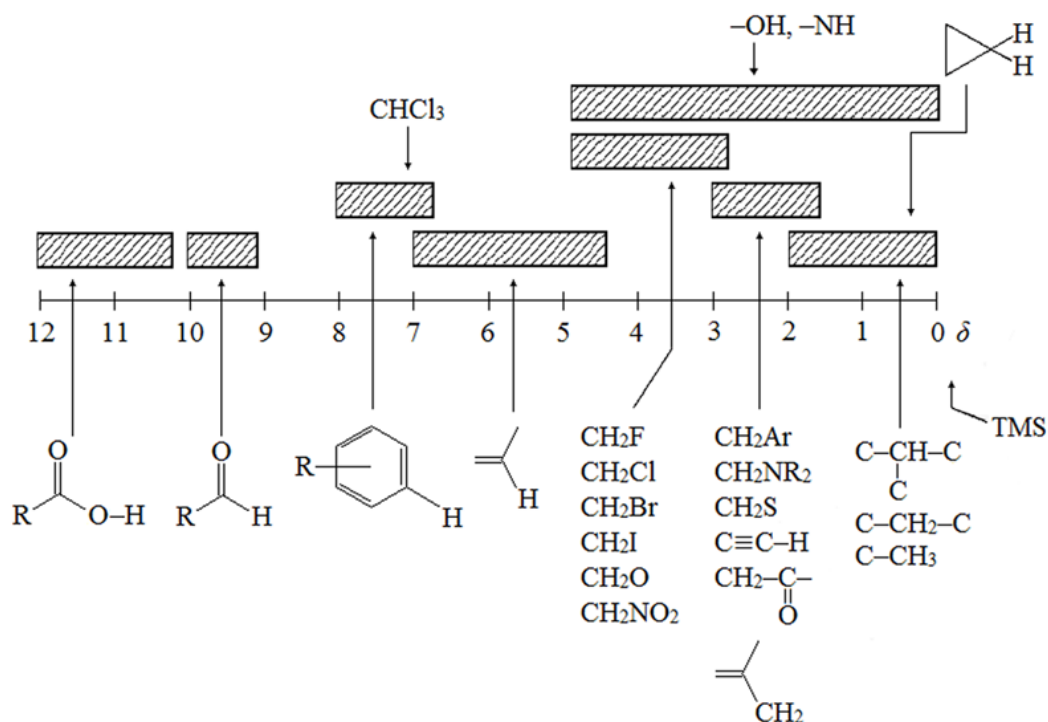


**Figure 2.15** A simplified correlation chart for proton chemical shift values (Pavia *et al.*, 1979).

On the other hand, the spectrum of  $^{13}C$ -NMR (Figure 2.17) reveals the number and type of carbon atom exist in a compound. Typically, the resonant frequency for carbon-13 is relatively lower than proton since it has a smaller magnetogyric ratio. The interpretation for  $^{13}C$ -NMR is simpler. Each carbon corresponds to a peak unless it is chemically equivalent. Basically, the correlation chart for carbon-13 are divided into few regions: saturated carbons without or with electronegative elements at lower chemical shifts, unsaturated or aromatic carbons at the middle region and finally carbonyl carbons at higher chemical shifts.



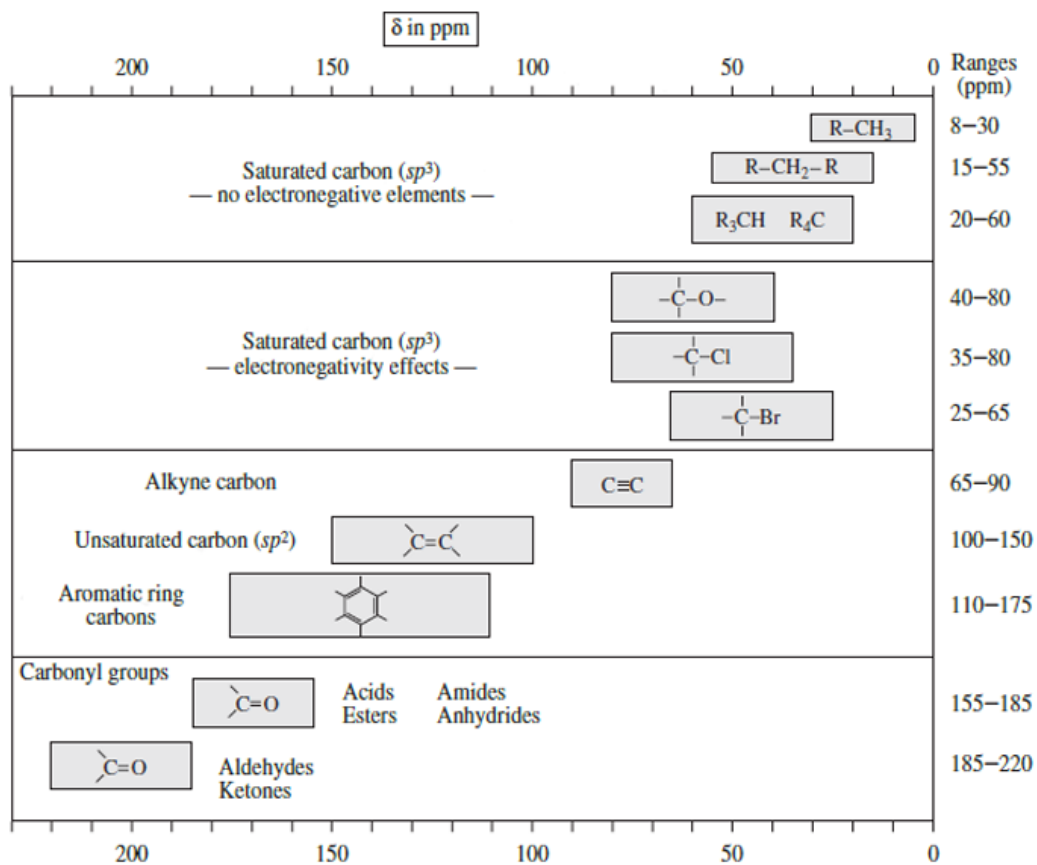


**Figure 2.16** A simple correlation chart for  $^{13}C$  chemical shift values (Pavia *et al.*, 1979).